

Large eddy simulation of a square cylinder flow: Modelling of inflow turbulence

M. Tutar[†]

Mersin University, Department of Mechanical Engineering, Çiftlikköy, 33343, Mersin, Turkey

I. Celik[‡]

*West Virginia University, Department of Mechanical and Aerospace Engineering,
Morgantown, WV 26506-6106, USA*

(Received April 4, 2007, Accepted October 26, 2007)

Abstract. The present study aims to generate turbulent inflow data to more accurately represent the turbulent flow around a square cylinder when the inflow turbulence level is significant. The modified random flow generation (RFG) technique in conjunction with a previously developed LES code is successfully adopted into a finite element based fluid flow solver to generate the required inflow turbulence boundary conditions for the three-dimensional (3-D) LES computations of transitional turbulent flow around a square cylinder at Reynolds number of 22,000. The near wall region is modelled without using wall approximate conditions and a wall damping coefficient is introduced into the calculation of sub-grid length scale in the boundary layer of the cylinder wall. The numerical results obtained from simulations are compared with each other and with the experimental data for different inflow turbulence boundary conditions in order to discuss the issues such as the synthetic inflow turbulence effects on the 3-D transitional flow behaviour in the near wake and the free shear layer, the basic mechanism by which stream turbulence interacts with the mean flow over the cylinder body and the prediction of integral flow parameters. The comparison among the LES results with and without inflow turbulence and the experimental data emphasizes that the turbulent inflow data generated by the present RFG technique for the LES computation can be a viable approach in accurately predicting the effects of inflow turbulence on the near wake turbulent flow characteristics around a bluff body.

Keywords: computational methods; random flow generation (RFG) algorithm; turbulence; large eddy simulation (LES); square cylinder; inflow turbulence.

1. Introduction

The turbulent flow field around bodies is of great practical importance because the results obtained in studying highly unsteady flow phenomena such as vortex shedding, can be applicable to the construction of high rise buildings, bridges, ocean marine piles and risers. Although the vortex shedding past a long square cylinder can be considered to be two-dimensional (2-D) and laminar at very low Reynolds numbers, at high Reynolds numbers, which are more relevant in practise, it can

[†] Corresponding Author, E-mail: m_tutar@mersin.edu.tr

be highly three-dimensional (3-D) and turbulent. Therefore, the computation of vortex shedding from the square section may require turbulence models in numerical studies and the turbulent flow measurements in the near wake of the cylinder should be conducted in the experimental studies at high Reynolds numbers.

Various experimental and numerical studies are conducted in the literature on the flow around square cylinders. Lyn and Rodi (1994), Lyn, *et al.* (1995), Saha, *et al.* (2000) experimentally investigated unsteady near wake flow features and the associated turbulent flow statistics. In numerical studies, much work is conducted in simulating 2-D flow around such bluff objects at moderate Reynolds numbers (Franke and Rodi 1991, Bouris and Bergeles 1999) and a few 3-D computations were also performed (Grigoriadis, *et al.* 2003). Turbulence modelling is always an important consideration of computational fluid dynamics (CFD) modelling of flow past bluff bodies at high Reynolds numbers, due to complex phenomena including the shear layer separation and the associated recirculation region, vortex shedding, and transition from laminar to turbulent flow regime, which is characterized by apparently highly fluctuations in flow quantities, both in space and time. In the literature, flow past square section cylinders are simulated numerically by different researchers based on different types of turbulence modelling ranging from Reynolds averaged Navier-Stokes (RANS) based turbulence models (Lee 1997, Franke and Rodi 1991) to LES (Sakamoto, *et al.* 1993, and Bouris and Bergeles 1999) to predict the turbulent vortex shedding from a square cylinder in comparison with the results of previous experimental studies (Lyn and Rodi 1994, and Lyn, *et al.* 1995).

Early numerical simulations with the RANS based turbulence models (Franke and Rodi 1991) suggest that the periodic vortex shedding pattern around a square cylinder can not be predicted realistically with the standard $k-\varepsilon$ turbulence model which completely ignores the unsteady boundary layer separation involved in periodic vortex shedding motion. The Reynolds Stress Equation (RSE) models on the other hand predict the correct level of total fluctuations and hence reproduce better integral flow parameter predictions such as vortex shedding frequency and the mean drag coefficient. However, Franke and Rodi (1991) demonstrated that even RSE models still have some problems in predicting this highly time dependent phenomenon as they are designed for flows that are steady in mean. Due to this fact, the latter numerical studies (Sakamoto, *et al.* 1993, Bouris and Bergeles 1999, Grigoriadis, *et al.* 2003) were conducted based on Large Eddy Simulation (LES) technique to investigate the flow around square cylinders even at low Reynolds numbers. These LES computations yield far more realistic results when compared to the results obtained from RANS computations. In the comparison of the results from various turbulence models it is also concluded that LES is not overly expensive in terms of computing time when compared to a realistic transient RANS simulation (Tutar and Holdo 2001). The numerical study conducted by Sakamoto, *et al.* (1993) in comparing results from two-dimensional simulations with three-dimensional simulations demonstrated that three-dimensional simulations further removes over conservatism from dynamic loading values whilst giving more realistic flow field predictions for LES.

Despite its superiority to RANS based turbulence models there are still some unresolved issues in LES applications to accurately resolve the turbulent flow around the bluff body. The treatment of velocity fluctuations at the inflow boundary i.e. the generation of inflow turbulence data is one of the most important issues. For the application of LES to a spatially developing, inhomogeneous turbulent flow, providing the in-flow boundary condition is a key aspect. In such cases, periodic boundary conditions can not be used as in fully developed flow cases like channels, (Akselvoll and Moin 1995) while the in-flow is always turbulent (Murakami, *et al.* 1999).

For high Reynolds number flows, inflow turbulence boundary condition becomes more significant and some method for generating turbulence inflow velocity fluctuations is required with a prescribed turbulence intensity value. In order to generate inflow turbulence, several different methods are suggested in the literature. One is to conduct a preliminary computation of a turbulent flow field using LES, such as a channel flow (Mochida, *et al.* 1992 and Murakami, *et al.* 1999) or a turbulent flow generated by a turbulence grid (Sakamoto, *et al.* 1990) and to store the time series of fluctuating velocity components for the inflow boundary conditions. This method may not be straightforward for the problems without well defined fully developed boundary layers and requires large computational resources and programming efforts. Furthermore, turbulence statistics from the preliminary calculations are not guaranteed to correspond to prescribed target characteristics as suggested by Kondo, *et al.* (1997). Spalart (1988) developed a very sophisticated approach in which a coordinate transformation is applied to the Navier-Stokes equations to enhance the capability of the method for spatially developing boundary layers. The coordinate transformation introduces new source terms to the Navier-Stokes equations that account for the inhomogeneity in the streamwise direction. Although the Spalart's method (1988) produces highly accurate inflow data, the procedure is somewhat complicated due to the evaluation of these terms. Therefore, Lund, *et al.* (1988) simplified the Spalart's method with a straightforward approach that transforms only the boundary conditions and not the entire solution domain. The result is a simple procedure where the velocity field from a plane near the domain exit is extracted, rescaled, and then reintroduced as an inflow boundary condition at the inlet of the domain.

Another method is to artificially generate time series of random velocity fluctuations by performing an inverse Fourier transform for prescribed spectral densities with specified turbulence intensities and length scales. There are two groups of approaches in this type of artificial turbulence generation method. One group uses the three-dimensional energy spectrum in the wave number domain obtained from spatial correlation of velocity as the target (Lee, *et al.* 1992, Rai and Moin 1993). This approach has the advantage of imposing the condition of continuity on the generation procedure without requiring the time series of velocity fluctuations to be stored, since the inflow turbulence is generated at each time step of LES computation. It was used with a varying degree of success by Lee, *et al.* (1992) for a simulation of compressible isotropic turbulence. However, for boundary layer flows, it is hard to prescribe the target three-dimensional energy spectrum as suggested by Kondo, *et al.* (1997) and this can be a major disadvantage of this approach for wind engineering flow applications. There are several other studies (Rai and Moin 1993, Bechara, *et al.* 1994) in this group of approach in the area of particle dispersion modelling based on generating an isotropic continuous flow field, as proposed by Kraichnan (1970). Another study conducted by Zhou and Leschziner (1991) complies with the latter requirement, but the resultant flow field does not satisfy the continuity condition and is spatially correlated. By pointing out the disadvantages of these applications, Celik, *et al.* (1999) suggested a relatively simple random flow generation (RFG) algorithm on the basis of the work of Kraichnan (1970) to account for the effects of anisotropy and inhomogeneity of turbulence. This algorithm involves scaling and orthogonal transformation operations applied to a continuous flow field generated as a superposition of harmonic functions and allows a realistic turbulent flow field, satisfying the continuity, anisotropy and inhomogeneity conditions, at a fraction of a cost of a solution of a full Navier-Stokes equations. The algorithm can be used as an efficient random flow field generator in LES in particle tracking. The work of Smirnov, *et al.* (2002) further extended the RFG technique of Celik, *et al.* (1999) and including a Lagrangian particle dynamic routine for efficient particle/bubble tracking in turbulent flows by satisfying mass-conservation of a fluctuating velocity field. In the second class of approaches,

power spectral density and cross-spectral density in frequency domain are obtained from time series of velocity fluctuations at the same point or two different points (Maruya and Morikawa 1994, Kondo, *et al.* 1996). Compared with the 3-D energy spectrum, these frequency spectra can be defined as targets with relative ease from measured data of boundary layer flow (Kondo, *et al.* 1997). Although that seems to be a very important advantage, the condition of continuity can not be imposed with that generation procedure. In addition, generated inflow turbulence must be stored before LES computation. This results in increased computer memory requirements for that approach

Near wall treatment is another important consideration in LES. A review of Rodi, *et al.* (1997), presenting the results of a workshop on LES computations of a bluff body, reveals that the LES approach with the use of “law of the wall” boundary conditions do not seem to be reliable enough to be used with confidence in separated flows, and the best treatment will be the use a sufficiently fine mesh in the vicinity of the wall to simulate the near wall flow with no slip condition. However, Murakami, *et al.* (1999) demonstrated the difficulty of using the no-slip boundary condition at solid walls when the Reynolds number is very high. Thus, some wall functions, such as Werner and Wengle type wall boundary conditions (Werner and Wengle 1991) may be necessary in bluff body flow problems. The study of Tutar and Holdo (2001) takes into account this fact for the transitional flow and suggests a near wall modelling methodology which combines no-slip boundary condition approach with van Driest’s mixing length approach to reduce the turbulent length scale in the vicinity of the cylinder wall up to some distance from the cylinder wall (2-8% of D), where the effects on the turbulence becomes negligible. The further study of Wakes, *et al.* (1999) focuses on LES of flow past a bluff body with a variety of different approaches that deal with flows around solid surfaces. In this numerical study, the simulations did not use any wall function, but a modified LES viscosity at the wall as suggested by Tutar (1998). The effect of changing the distance of the first mesh element from the wall was also studied.

The present numerical study attempts to improve the 3-D LES predictions for turbulent flow past a square cylinder with the use of the random flow generation (RFG) algorithm for generating turbulent inflow boundary condition data for LES when the inflow turbulence level may be significant. The wall effects are taken into consideration by reducing the sub-grid length scale in the boundary layer region with the use of a near wall modelling methodology which combines the no-slip wall boundary condition approach with van Driest’s mixing length function (van Driest 1956) to capture the turbulence effects for the present transitional flow. The effects of different inflow boundary conditions on predicting dynamic loading of a smooth square cylinder at a Reynolds number of 22,000 is investigated. At such Reynolds number the flow may be transitional and it is necessary to include a turbulence model to simulate the effects of turbulence in the near wake of the cylinder after separation.

2. Mathematical model

2.1. Sub grid-scale closure

Applying a filtering process to the Navier-Stokes equations and continuity equations results in the following governing equations

$$\frac{\partial}{\partial t}(\rho \bar{u}_i) + \frac{\partial}{\partial x_j}(\rho \bar{u}_i \bar{u}_j) = \frac{\partial}{\partial x_j} \left(\mu \frac{\partial \bar{u}_i}{\partial x_j} \right) - \frac{\partial \bar{p}}{\partial x_i} - \frac{\partial \tau_{ij}}{\partial x_j} \quad (1)$$

$$\frac{\partial \rho}{\partial t} + \frac{\partial \rho \bar{u}_i}{\partial x_i} = 0 \quad (2)$$

where ρ is the fluid density, μ is the dynamic viscosity of the fluid, \bar{u}_i is the filtered value of the velocity, \bar{p} is the filtered value of the pressure, and $\tau_{ij}(\rho \bar{u}_i \bar{u}_j - \rho \bar{u}_i \bar{u}_j)$ is the sub-grid scale stress. To close the filtered equations the sub-grid scale stress is modelled using a viscous analogy. The sub-grid scale stress can thus be expressed as

$$\tau_{ij} = -2\mu_t \bar{S}_{ij} + \frac{2}{3} k_{sgs} \delta_{ij} \quad (3)$$

where k_{sgs} is the sub-grid scale kinetic energy, $\bar{S}_{ij} (1/2(\partial \bar{u}_i / \partial x_j + \partial \bar{u}_j / \partial x_i))$ is the strain rate tensor of the resolved flow field and μ_t is the sub-grid scale viscosity term calculated by the Smagorinsky model (Smagorinsky 1963) given as

$$\mu_t = \rho (C_s \Delta)^2 (2\bar{S}_{ij} \bar{S}_{ij})^{1/2} \quad (4)$$

With C_s is the Smagorinsky constant and Δ is the representative characteristic sub-grid length scale given by

$$\Delta = (\Delta_x \Delta_y \Delta_z)^{1/3} \quad (5)$$

Therefore the sub-grid length scale is calculated directly from the local grid size and the grid size distribution is thus very important for the present sub-grid scale (SGS) model. The calculation of the sub-grid scale viscosity is performed using a subroutine that returns an array of values at each integration point of the finite element in the computational domain at each time step. All numerical simulations are conducted with a Smagorinsky constant of $C_s = 0.10$, as suggested value Sakamoto, *et al.* (1993) for practical applications of the 3-D LES computations of turbulent flows around a square obstacle.

2.2. Generation of turbulent inflow data

In the present study, in order to generate a realistic random inflow flow generation (RFG), a modified version of Kraichnan's technique (Kraichnan 1970) is proposed. The present random flow generation technique which is previously developed by Celik, *et al.* (1999) and further extended Smirnov, *et al.* (2002) is incorporated into the LES approach in the finite element solver (Fluent 1993). The RFG algorithm can be used to prescribe inlet conditions as well as initial conditions for spatially developing inhomogeneous, anisotropic turbulent flows (Smirnov, *et al.* 2000). When the RFG algorithm is used for LES the fluid particles should follow a time-dependent flow-field and fluctuating component should still be added to it at smaller turbulent scales (Smirnov, *et al.* 2000). The fluctuating component is derived from the turbulence intensity and length-scales, provided by the turbulence model or via empirical relations. In this procedure adopted here a homogeneous isotropic transient flow field is realized as a superposition of harmonic functions as previously suggested by Kraichnan (1970):

$$\vec{v}(x, t) = \sqrt{\frac{2}{N}} \sum_{n=1}^N [\vec{v}_1(\vec{k}_n) \text{Cos}(\vec{k}_n \cdot \vec{x} + \omega_n t) + \vec{v}_2(\vec{k}_n) \text{Sin}(\vec{k}_n \cdot \vec{x} + \omega_n t)] \quad (6)$$

In this equation,

$$\vec{v}_1(\vec{k}_n) = \vec{\zeta}_n x \vec{k}_n, \quad \vec{v}_2(\vec{k}_n) = \vec{\zeta}_n x \vec{k}_n, \quad (7)$$

with

$$\vec{k}_n \cdot \vec{v}_1(\vec{k}_n) = \vec{k}_n \cdot \vec{v}_2(\vec{k}_n) = 0 \quad (8)$$

where the components of vectors $\vec{\zeta}_n$ and $\vec{\zeta}_n$ and the frequency ω_n are chosen independently from a Gaussian distribution with a standard deviation of unity, $N(0,1)$. Each component of \vec{k}_n is a Gaussian random number with a standard deviation of 1/2. Here, N is the number of terms in series. The generated flow-field is then homogeneous, isotropic and divergence-free (Smirnov, *et al.* 2000).

The RFG algorithm utilized here is realized in 3-D manner using a subroutine written in a hybrid code language. For this purpose, the subroutine, which is located in the present LES code for the imposition of velocity boundary conditions performs calculation of velocity fluctuations in accordance with a proper selection of length and time scales for the turbulence conditions and then returns the calculated values of fluctuating velocity components at each grid point of the inflow boundary at each time step.

3. Mesh configuration and numerical details

The geometry considered for all 3-D simulations and the corresponding velocity boundary conditions are shown in Fig. 1. The flow is described in a Cartesian coordinate system (x, y, z) , in which the x -axis is aligned with the streamwise direction, the z -axis is parallel with the spanwise direction or the cylinder axis and the y -axis is perpendicular to both directions, as shown in Fig. 1. A stationary 3-D square cylinder with a side length, D is situated in the centre of the vertical plane and is exposed to a time- and spanwise-averaged free stream velocity, U . The Reynolds number based on the free stream velocity and the cylinder diameter is 22,000. Inlet (upstream), upper and lower boundaries are extended laterally to minimize the effects of the boundaries on the cylinder. In the present study there are also no boundary layers on the side walls of the flow domain (boundary layers are of course present on the wind tunnel walls) due to the symmetry boundary conditions; thus the effect of blockage is less than for a typical experimental case. The flow domain is also extended long enough downstream to eliminate the far field effects on the near wake and to produce full development of the vortex street. The simulations are carried out for the mesh resolution of $365 \times 209 \times 32$, $365 \times 209 \times 48$ grid points in the (x, y, z) direction for 3-D simulations and 365×209 and 265×209 grid points in the (x, y) direction for 2-D simulations to study the effect of mesh resolution on the flow results. The 3-D plane view of the $365 \times 209 \times 32$ mesh system used for the present study is illustrated in Fig. 2. The computational domains contain grid points which are non-uniformly spaced in the x - and y -. Extremely high mesh resolution is used between the inflow boundary and the front face of the cylinder to ensure that the inflow turbulence effects are able to reach the cylinder. Very fine mesh resolution was used at the vicinity of the cylinder. The mesh size is increased with the distance from the cylinder surface and the location of the first grid point from the cylinder wall is chosen to be 0.12 per cent of the cylinder diameter. Mesh space is stretched using geometric progression function with expansion factors in the streamwise and lateral directions. On the other hand, equally distributed grid points are used in the spanwise direction in which the length of the computational domain is not so large so that our attention is restricted to eddies that

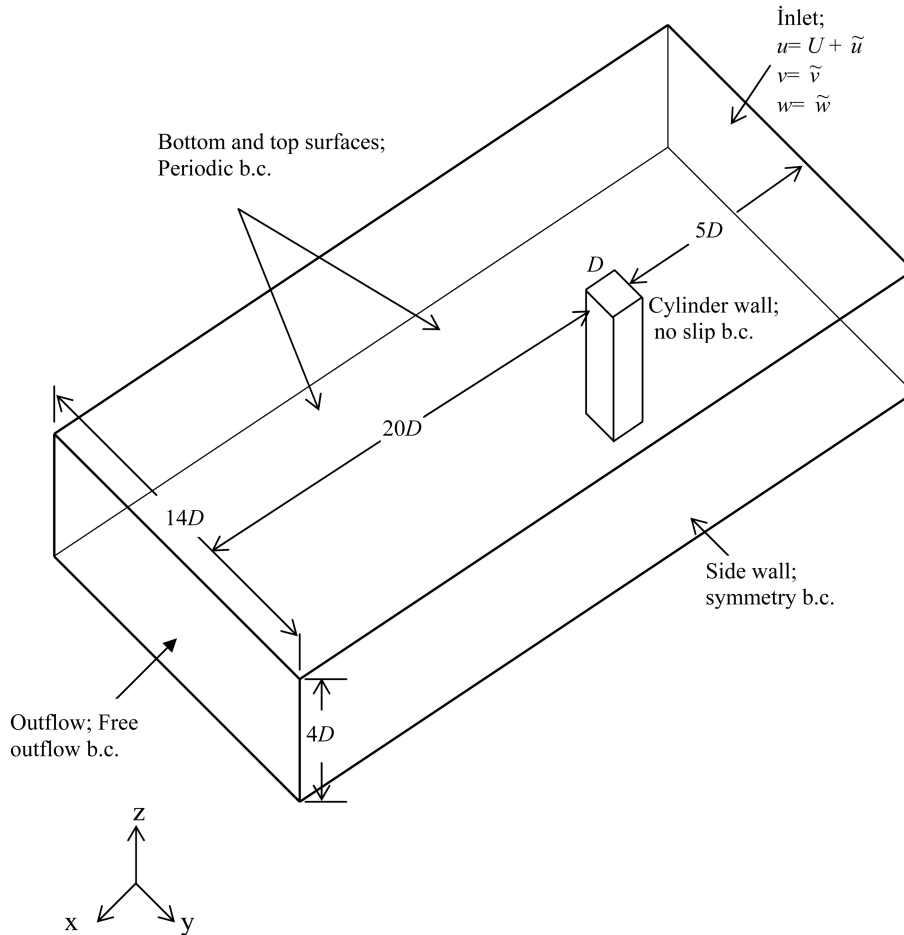


Fig. 1 The geometric configuration of the flow domain and the velocity boundary conditions. The fluctuating velocity components (\tilde{u} , \tilde{v} , \tilde{w}) at the inflow boundary are computed by the RFG algorithm and are superimposed on the time averaged velocity values

are small compared to the diameter of the cylinder. All simulations are carried out using a finite element solver (Fluent 2003). The whole computational domain is subdivided into a finite number of small three dimensional eight-noded brick elements. The non-linear equation systems resulting from the finite element discretization of the flow equations are solved using a segregated solution algorithm with a second-order trapezoid time integration scheme in each finite element so that the advection terms have a higher order of accuracy in order to improve numerical stability. All fluid properties including density and the dynamic viscosity, are assumed constant, while the non-dimensional time step, Ut/D had a constant value of 0.01. The convergence criteria is set to 0.001 for all simulations. All integral variables are made non-dimensional by using U and D . In the present study all simulations are carried out by considering the following velocity boundary conditions:

1. Inflow boundary: Random velocity fluctuations generated by the RFG technique are superimposed on the corresponding velocity components. The time- and spanwise-averaged streamwise velocity

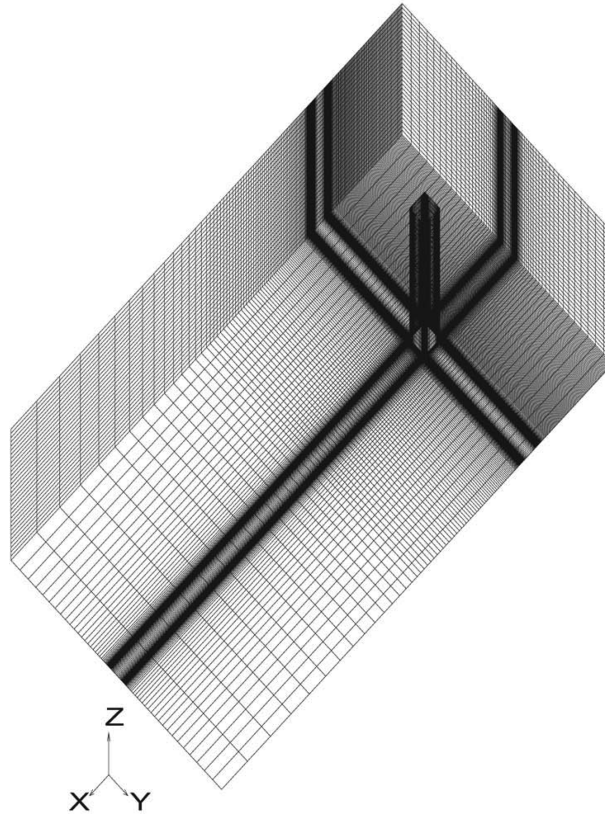


Fig. 2 Global 3-D computational mesh ($365 \times 209 \times 32$ grid points) used for the present LES calculations

component is assumed to be uniform, ($\langle u \rangle_{tz} = U$) while other velocity components are assumed to be zero ($\langle u \rangle_{tz} = \langle w \rangle_{tz} = 0$)

2. Outflow boundary: Free out flow boundary conditions are imposed. Diffusion fluxes for all flow variables in the direction normal to the exit plane are assumed to be zero

3. Top-bottom boundaries: Periodic boundary conditions at the top and bottom boundaries are used to simulate a small portion of the infinitely long cylinder

4. Lateral boundaries: Symmetric boundary conditions at the transverse boundaries are applied in order to take into account for the fact that only a small portion of of an infinite domain is modelled. The normal velocity components and the normal gradients of all velocity components are assumed to be zero.

5. Cylinder surface: no-slip velocity boundary condition is prescribed at the cylinder surface. A near wall methodology which comprises the no-slip velocity boundary condition and a damped mixing length model is used to simulate the flow in the vicinity of the cylinder surface.

With the application of the near wall methodology in the present study, wall effects are taken into consideration by reducing the sub-grid length scale, l in the boundary layer up to some point from the cylinder wall, where the effects on the turbulence become negligible (Tutar 1998). In order for the near wall Methodology to perform satisfactory, the boundary layer is resolved by extremely high mesh density. A damping function D_f is introduced to reduce the sub-grid length scale up to 8 percent of the cylinder length from the cylinder and is calculated by an alternative form of van

Driest's function (van Driest 1956) as follows:

$$D_f = [1 - \exp(-y^+/25)^3]^{1/2} \quad (9)$$

Where A^+ is a constant for which a value of 25 is used. The above formula has the property of yielding not only $l=0$, but also $\partial l/\partial y = 0$ on the wall. This may be preferable for numerical reasons (e.g. to avoid sharp gradients of l). Thus by taking wall effects into account, the sub-grid length scale is recalculated ($l = C_s A D_f$) in the near wall region. The turbulent inflow data are generated with use of integral turbulence length scale and turbulence intensity. The normal stress components are prescribed at the inflow boundary based on the isotropic turbulence intensity values varying from 0 to 10 percent. The turbulence length scale on the other hand is computed from the Boussinesq-eddy viscosity relation based on a value of eddy-viscosity ratio of $\nu_t/\nu = 10$ which corresponds better with the experiment of Lyn, *et al.* (1995) according to the recommendations of the former studies of RANS simulations (Bosch and Rodi 1995).

4. Results and discussions

The influence of turbulent inflow data on the vortex shedding mechanism and hence on the integral flow predictions is extensively studied to assess the functionality of the suggested RFG technique or the present LES approach and to constitute a better mechanism for the treatment of velocity fluctuations at the inflow boundary in future LES calculations of bluff body flows. With this regard, the role of the present RFG technique in the present LES study is investigated for different turbulent inflow boundary conditions i.e. varying degree of turbulence at a Reynolds number of 22,000 to compare the numerical results with those obtained from the well-known experimental studies of Lyn, *et al.* (1994 and 1995) in which the free stream flow velocity was 0.533 m/s with an upstream turbulence intensity of 2 %. The simulations are conducted in 3-D manner as the turbulent vortex shedding from the cylinder is considered to be 3-D and the vortex stretching mechanism plays a major role in determining the near wake turbulent flow characteristics. In order to show the necessity for the present 3-D computations for LES, 2-D simulations are also carried out. For the 2-D case the same code, solver-set up, the cross-sectional grid and turbulence modelling parameters are used in order to make the results comparable.

4.1. Primary flow features and statistics: Comparison between 2-D and 3-D results

The turbulent flow past a square cylinder at high Reynolds numbers represents complex behaviours with the presence of periodic vortex shedding from the front corner of square cylinder which introduces a low-frequency variation of the velocity field behind the cylinder in addition to the high-frequency turbulence fluctuations (Bouris and Bergeles 1999). There are a few basic mechanisms that may be identified for such flows: transition to turbulence in shear layers, interference of separated shear layers with the sides of the cylinder and the enhanced mixing and entrainment of the fluid from the base region of the cylinder when the inflow turbulence effects are increasing. There have been claims that large eddy simulations should only be performed in three dimensions since the 2-D computations are inferior to 3-D computations to accurately represent the 3-D characteristics of turbulent structures in the near wake of the cylinder. Bearing this in mind, in the present study the formation and shedding of vortices in the near wake of the cylinder are studied with 3-D LES computations by considering different turbulent inflow boundary conditions. Basic flow features

such as transition to turbulence in shear layers, vortices developing from the leading edge of the square cylinder, the reverse flow characteristics and the pressure distribution along the side faces and the von Karman type vortex street with periodic vortex shedding are observed for each simulation. For brevity, only those obtained from 2-D and 3-D simulations conducted at turbulence intensity of 2 percent are presented to study basic flow features and the effect of mesh resolution and the dimensionality of turbulence modelling on these features and the integral flow parameters in this section.

Figs. 3 (a)-(d) show the instantaneous vorticity contours and velocity vectors obtained from the 2-D and 3-D simulation at mid-spanwise locations during the development of the free shear layers from the both sides of the square cylinder at an early non-dimensional simulation time. The formation of separated shear layers from the leading edges of the square cylinder and the simulated size of the reverse flow region near the side faces of the cylinder show differences for 2-D and 3-D computations. As can be easily seen from instantaneous vorticity contours taken at non-dimensional time of 5 in Figs. 3 (a) and (b), the separated shear layer in the case of the 3-D simulation (Case 4) is found to extend to a larger streamwise distance compared to the 2-D simulation (Case 2). The more elongated shear layer as an indication of the weaker vortex shedding process into the near wake of the cylinder gives a longer time averaged recirculation region behind the cylinder in 3-D simulation leading to a smaller drag coefficient compared to the 2-D simulation as summarized in Table 1. This is mainly due to the fact that in 3-D computations the interaction of separated shear layers which are basically unstable become more intense related to the extent of entrainment of fluid into the free shear layers and the increasing turbulent viscous diffusion in association with 3-D mixing effects at this high Reynolds number. The entrainment of fluid from the base region of the cylinder due to intense interaction of the free shear layers and the presence of the rear corners which interfere with the development of these highly curved free shear layers weaken the vortex shedding process leading to the increasing the base pressure and thus reducing the drag for the 3-D computations compared to the 2-D computations. Figs. 3(c) and (d) also show instantaneous velocity vectors obtained from both 2-D and 3-D simulations for a comparison of the reverse flow region and eddies of varying scales in it along the side face of the cylinder. Although both computations show the existence of the flow region near the side faces, the 3-D computations produce smaller reverse flow region compared to the 2-D computations. As a result, a more complete pressure recovery towards the rear of the sides of the cylinder is expected for 3-D computations compared to 2-D computations.

As the wake further develops the large vortices slowly shift away from the cylinder due to their self-induced velocity fields and the instabilities originating from the rounding errors and numerical dispersion in addition to the upstream effects lead the flow to eventually become asymmetric. The instantaneous vorticity contours obtained from 2-D and 3-D cases of different 2-D planes in the wake of the cylinder are observed in Figs. 4 (a)-(c) at a non-dimensional time of $t^* = 38$. The vorticity patterns obtained from the 3-D case indicate that some random small-scale structures appear in the near wake of the cylinder in the large scale structures as illustrated in the x - y plane at a mid-spanwise location of $z/D = 2$ in Fig. 4 (b). The different flow patterns observed in the different spanwise locations for the 3-D computations as seen in Figs. 4 (b) and (c) can be also attributed to the existence of vortex stretching mechanism and hence the lack of two-dimensionality in the present computations. In contrast to the 3-D simulation, the 2-D simulation can not reproduce these small scale eddies which interact with the large scale Karman vortices as seen in Fig. 4 (a). This is probably due to highly turbulent and 3-D flow structures in the wake region and the inability of 2-D

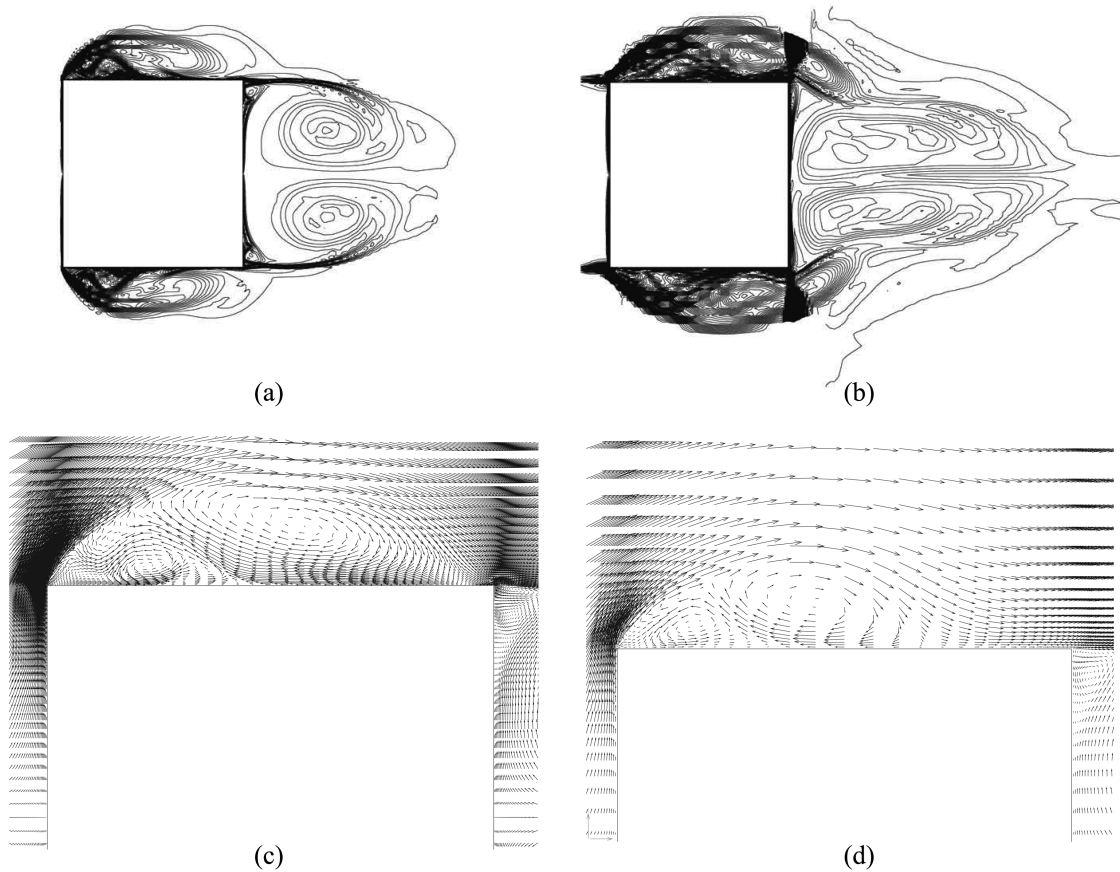


Fig. 3 The instantaneous vorticity contours and velocity vectors obtained from 2-D and 3-D LES computations in the x - y plane at $z/D = 2.0$ at early non-dimensional times at inflow turbulence level of 2 percent; a) 2-D computation (Case 2) at $t^* = 9.2$; b) 2-D computation (Case 4) at $t^* = 9.2$; c) 2-D computation (Case 2) at $t^* = 13.2$; d) 3-D computation (Case 4) at $t^* = 13.2$

simulation in capturing these small scale structures. However, such a vortex-street-like structure (the well-known von Karman vortex street) with periodic vortex shedding is discernable in 2-D case and the more pronounced asymmetric vortex shedding mechanism obtained from 2-D case. The vortices starting from the front corners of the cylinder become stronger and roll-up more into the near wake of the cylinder for the 2-D computation compared to the 3-D counterpart. Therefore, the simulated strength of the large vortices is found to be stronger for the 2-D case than for the 3-D case and hence the stronger vortex shedding mechanism lead to the increased mean and fluctuating parts for the force coefficients for 2-D case as summarized in Table 1. The instantaneous velocity vectors at the mid-transverse plane ($y/D = 7$) presents the fluctuating velocity field as an indication of unstable flow in the wake as seen in Fig. 4 (d). The vortex shedding period is determined using the power spectral density of the vorticity generation at a point $(x, y, z) = (6.5D, 7D, 2D)$ in the near wake of the cylinder and is presented in Table 1. The predicted non-dimensional vortex shedding frequencies are 0.135 and 0.137 for 3-D and 2-D computations respectively while the experimental study produces 0.132 for the non-dimensional vortex shedding frequency. The large deviations between

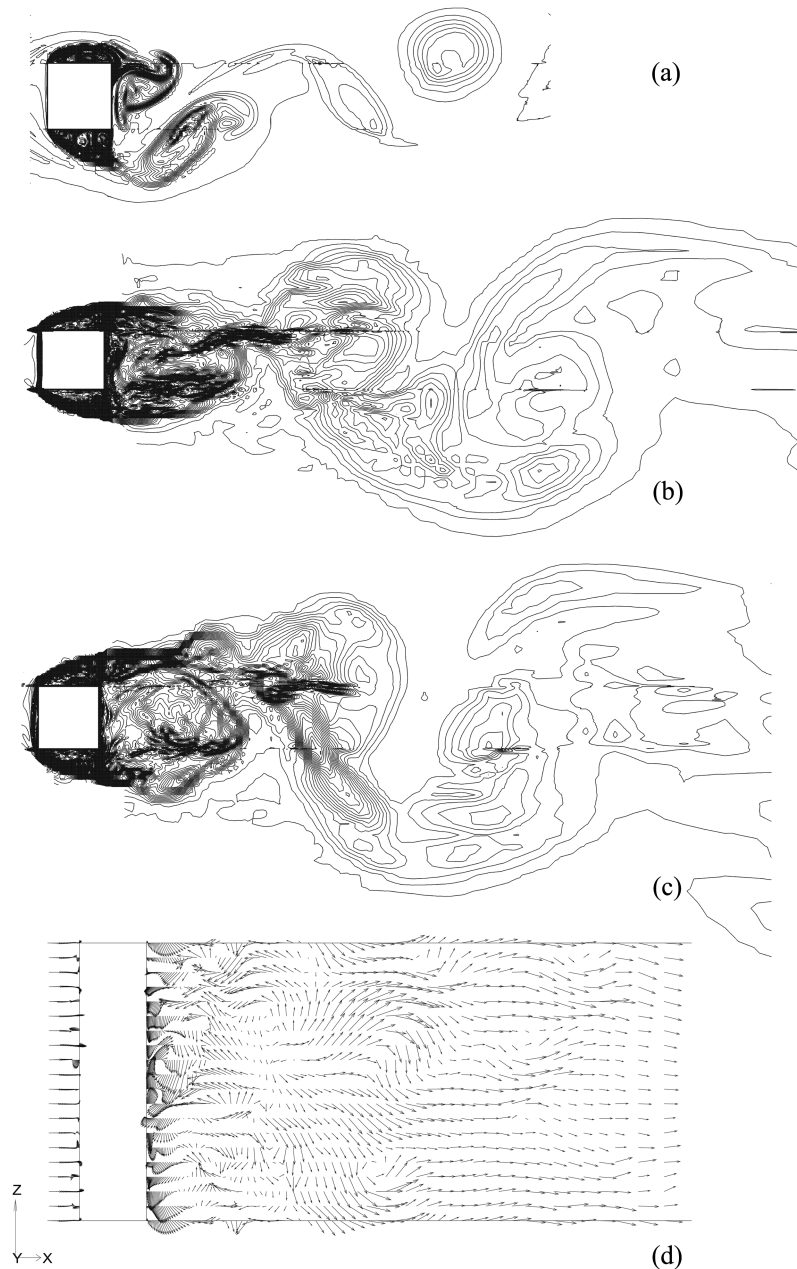


Fig. 4 The instantaneous vorticity contours and velocity field obtained from 2-D and 3-D LES at a non-dimensional time of $t^* = 38$ at inflow turbulence level of 2 percent; a) Case 2; b) Case 4, 2-D view in the x - y plane at $z/D = 2$; c) Case 4, 2-D view in the x - y plane at $z/D = 1.5$; d) Case 4, 2-D view in the x - z plane at $y/D = 7$

the 2-D and 3-D results indicate that highly turbulent 3-D structures strongly influence the near wake flow characteristics and hence the predictions of the integrated force coefficient calculations. The application of the present RFG algorithm seems to slightly improve the 2-D results as

Table 1 Overview of calculated integral parameters at $Re = 22,000$

| Simulation | Turbulent Inflow Data (Iu isotropic turbulence intensity) | Mesh Resolution | \bar{C}_D | \tilde{C}_L | L_r/D | \bar{C}_{Pb} | St_v |
|------------|--|----------------------------|-------------|---------------|---------|----------------|--------|
| Case 1 | 2 % | 265×209 | 2.34 | 1.39 | 0.83 | -1.91 | 0.137 |
| Case 2 | 2 % | 365×209 | 2.31 | 1.31 | 0.92 | -1.88 | 0.137 |
| Case 3 | 2 % | $365 \times 209 \times 32$ | 2.21 | 1.16 | 1.25 | -1.77 | 0.134 |
| Case 4 | 2 % | $365 \times 209 \times 48$ | 2.14 | 1.10 | 1.30 | -1.68 | 0.135 |
| Case 5 | 10 % | $365 \times 209 \times 48$ | 1.91 | 0.79 | 1.46 | -1.41 | 0.144 |
| Case 6 | Smooth inflow | $365 \times 209 \times 48$ | 2.23 | 1.21 | 1.27 | -1.81 | 0.133 |
| | Experiment (Lyn, <i>et al.</i> 1994,1995 $Iu = 2\%$ isotropic turbulence) | | 2.10 | - | 1.38 | | 0.132 |

illustrated in Table 1. However, much better agreement between the experimental data and the 3-D results are observed.

Long time-averaged results for velocity statistics along the centreline are obtained from all simulation cases and are presented in Fig. 5. The time averaging is applied to the LES calculations for a period of 12 shedding cycles at the end of the each simulation. It is found that time averaging over 12 shedding cycles is sufficient to achieve statistical steady state of the near wake turbulence for 3-D calculations. Fig. 5 displays the distribution of the time-and-spanwise-averaged streamwise velocity component, $\langle u \rangle$ for different mesh resolutions along the centerline and provides information on the length of the time-averaged recirculation length (L_r/D) behind the cylinder. Experimental data of Lyn, *et al.* (1994) are also included. It is clearly seen in Fig. 5 that there are fairly large differences between the 2-D and 3-D computations in the very near wake region ($1 < x/D < 2.5$). The 2-D computations considerably underestimate the length of the reverse flow region in comparison with the 3-D computations and the experimental data. On the other hand, the results of the 3-D computations significantly improves the accuracy and shows much better agreement with the experimental data in the very near-wake region of the cylinder. The basic reason of this large discrepancy between the 2-D and 3-D computations is due to the three dimensionality of the near wake which determines the wake characteristics. Specifically, the vortex stretching mechanism is intense in the near wake region where all the three components of the vortices are present as shown in Figs. 4(c) and (d). The vortex stretching mechanism weakens the strength of the large vortices in the near wake region due to strong interaction between the separated shear layers and hence long-stretched separated shear layers resulting in increasing base pressure are obtained from the 3-D computations. The increase in the mesh resolution in the streamwise direction further improves the prediction of the velocity as seen in Fig. 5. In addition to the differences in the calculated values of the recirculation length as observed in Table1, the 2-D and 3-D computations also predict different maximum reverse flow intensity in the recirculating region. The magnitude of reversed velocity for the 3-D computations seems to agree with the experimental data slightly better than that of the 2-D computation. Further downstream ($x/D > 3$), although the 3-D computations with the high mesh resolution in the streamwise direction seems to give a more accurate velocity distribution than the 2-D computations, the recoveries of the streamwise velocity in all simulation cases are more rapid than that in the experiment (the asymptotic value of the predicted streamwise velocity is higher than the experimental observation). The better predicted velocity distribution for the 2-D computations with the higher mesh resolution also reveals that fine mesh resolution in the 2-D plane is still very important for such flow solutions. As the mesh resolution of $365 \times 209 \times 48$ grid points (Case 4)

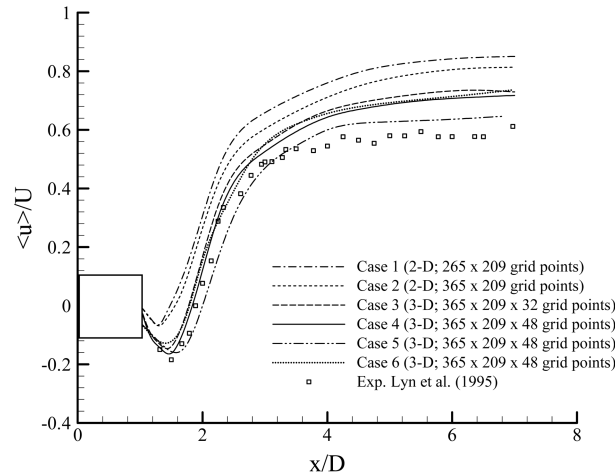


Fig. 5 The distributions of time-and-spanwise -averaged streamwise velocity component, $\langle u \rangle / U$ for different mesh resolutions along the centreline

shows the better agreement with the experimental data compared with the other mesh systems tested at inflow turbulence intensity of 2 percent, this mesh system is adopted for all subsequent computations of the present study. Fig. 5 also demonstrates the effect of varying inflow turbulence intensity on the present flow as well as the effect of mesh resolution.

4.2. The effect of inflow turbulence data

The influence of generated turbulent inflow data on the present flow is extensively investigated for different turbulence intensities for a final decided mesh system of $365 \times 209 \times 48$ grid points. For this purpose, numerical simulations are performed in conjunction with the RFG algorithm to generate the isotropic inflow turbulence of which the turbulence level is varied from 2 to 10 percent. Figs. 6 (a) and (b) show the velocity components (u , v , w) variations with respect to time at the inflow boundary at two different locations for varying degree of inflow turbulence (Cases 4 and 5). All velocity components are non-dimensionalized with respect to the time-averaged streamwise velocity component defined at the inflow boundary. The variations in the velocity components clearly demonstrate the effect of turbulence on flow at the inflow boundary. The frequency and amplitude of the velocity fluctuations increase as the inflow turbulence level is increased from 2 to 10 percent. The spatial variations (i.e. phase lag) observed in the history of each velocity component at two different points as seen in Fig. 6 (a) can be attributed to spatial inhomogeneity that should be satisfied at the inflow boundary for realistic flow simulations. The present RFG algorithm therefore ensures the spatially evolving isotropic turbulence along the inflow boundary.

The corresponding one-dimensional energy spectrums of y velocity component for different inflow turbulence conditions at three different locations along the centreline of the cylinder are computed. The energy spectrums are non-dimensionalized with respect to the total energy in each case, and are plotted with respect to the non-dimensional vortex shedding frequency fD/U , where f is the frequency, U is the time averaged streamwise velocity at the inflow boundary and D is the cylinder side length. The energy spectrum of the y velocity perturbation is calculated using a method based on a Fourier transformation approach as follows:

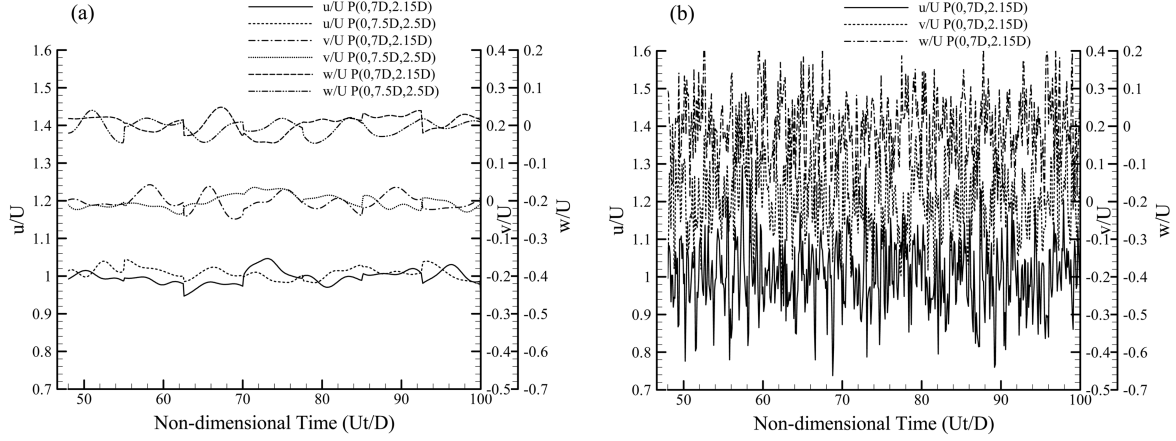


Fig. 6 The time history of non-dimensional x and y velocity components for the 3-D LES computations at two different points $P(0, 7D, 2.15D)$ and $(0, 7.5D, 2.5D)$ at the inflow boundary for different turbulence inflow boundary conditions generated by the RFG algorithm; a) Case 4 at $I_u = 2\%$; b) Case 5 at $I_u = 10\%$

$$S_1(\omega_n) = E \left[\frac{h_T}{M_d} \left| \sum_{m=1}^{M_d} U'_1(t_m) \exp(-i\omega_n t_m) \right|^2 \right]_{N_d} \quad (10)$$

$(n = 1, \dots, M_d)$

where $\omega_n = 2\pi n/(h_T M_d)$ is the non-dimensional circular frequency, M_d is the number of time series data, $E[*]_{N_d}$ denotes the averaging over N_d samples. In the present study, about 8500 samples at each location of streamwise velocity component are collected over a time interval Ut/D of 90. The energy spectrum can then be converted into wave number domain as,

$$E_1(\alpha_n) = U_c S_1(\omega_n) \quad (11)$$

where $\alpha = \omega_n/U_c$ is the wave number.

Figs. 7 (a)-(c) show the energy spectrums at three different locations along the centreline of the cylinder for these cases (Cases 4-6). Fig. 7 (a) shows the energy spectrum at a point $P(0, 7D, 2D)$ at the inflow boundary for isotropic inflow turbulence of 2 and 10 percents. While the energy spectrum is confined to a narrow band for Case 4 a broader banded energy spectrum is obtained for Case 5. However, both cases can capture the inertial sub-range as observed in Fig. 7 (a). Fig. 7 (b) shows the energy spectrums for three different cases including the smooth inflow case very near to the front stagnation point of the cylinder. The small velocity fluctuations generated by the RFG algorithm at low inflow turbulence intensity of 2 percent are able to distort the mean flow in the stagnation region and a good portion of the inertial sub-range can be captured here. The energy spectra for the y velocity component appear to exhibit an inertial sub-range about a half decade of inertial sub-range from about non-dimensional frequency of 1.5 to 10 where energy spectra exhibit a slope close to $-5/3$ predicted by Kolmogorov theory. The energy spectrum determined at point $P(6.5D, 7D, 2D)$ in the very near wake of the cylinder can be also seen in Fig. 7 (c). Most of the energy is contained at the larger frequencies compared to the near front stagnation point spectrum.

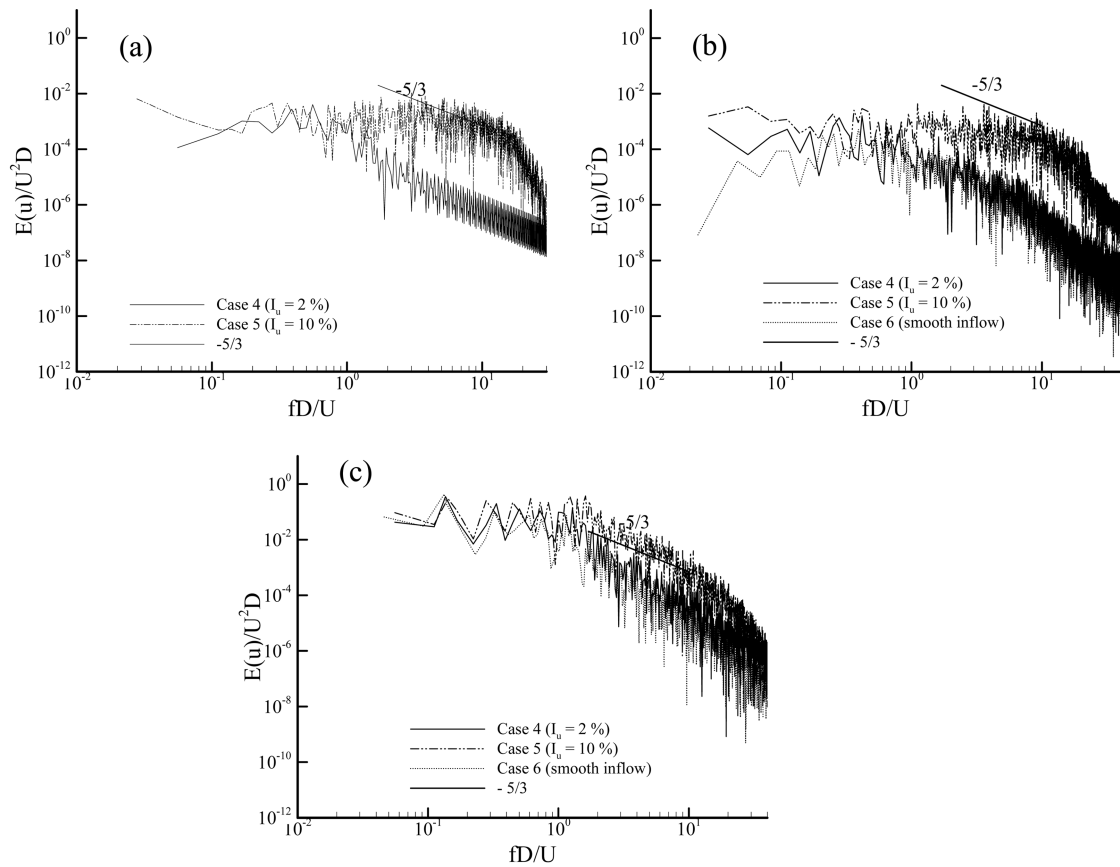


Fig. 7 One-dimensional energy spectrums for the y velocity component obtained from the 3-D LES computations at selected three different locations along the centreline of the cylinder for different turbulent inflow data; a) $P(0, 7D, 2D)$ inflow boundary ; b) $P(4.985D, 7D, 2D)$ very near to the front stagnation point of the cylinder; c) $P(6.5D, 7D, 2D)$ in the near wake location; $-5/3$ slope

The broader banded distribution of the energy at this in-wake location compared to that at the selected front stagnation point for each case can be attributed to the occurrence of the near wake turbulence and the associated large irregular wake velocity fluctuations. The dominant frequencies representing the non-dimensional vortex shedding frequencies are also noticeable in Fig. 7 (c) for each case. Increase in the turbulence intensity increases the non-dimensional vortex shedding frequencies. This is due to the fact that intense interaction of separated shear layers occur behind the cylinder and this leads to earlier roll-up and cut-off of vortex sheet resulting in higher vortex shedding frequency. The peak values are also found to be less pronounced as the turbulence intensity increases. This is probably due to the fact that as the turbulence intensity increases the vortex shedding process is mainly governed by the strong turbulent fluctuations resulting in a smaller spectral density of vortex shedding and larger spectral density of turbulent fluctuations at higher frequencies as seen in Fig. 7 (c). It is also illustrated in Fig. 7 (c) that when the isotropic turbulence intensity is increased to 10 percent (Case 5) the energy spectrum shows more energy at the larger frequencies in the inertial sub-range and the distribution of the energy is much broader banded. Simulations with the RFG algorithm show a slightly slower decay of the energy spectra and

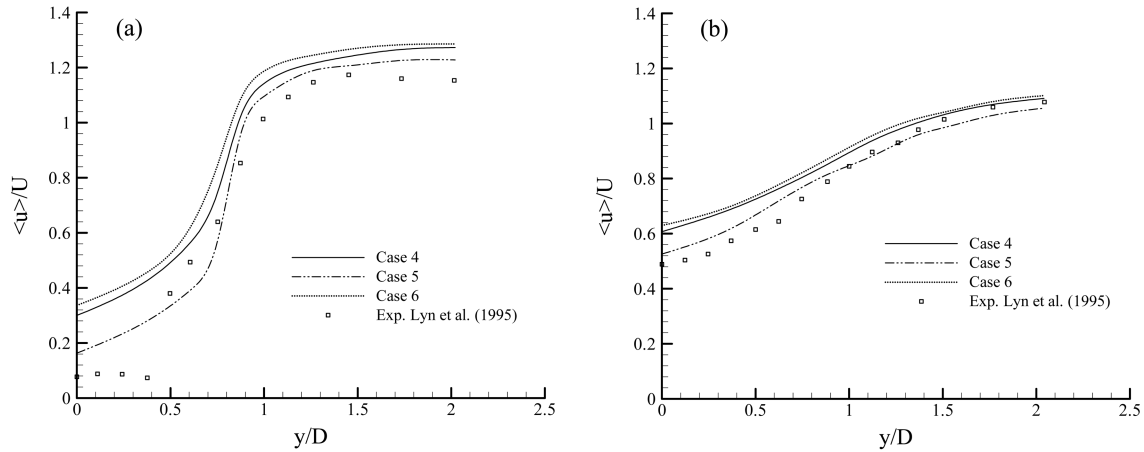


Fig. 8 The time-averaged profiles of streamwise velocity component at two different downstream locations in the near wake for different inflow turbulence data; a) Streamwise velocity component at $x/D = 1.5$; b) Streamwise velocity component at $x/D = 2.5$

more energy at the high frequencies with increasing turbulence intensity.

Effects of inflow turbulence on the wake flow characteristics in terms of the long-time averaged results of streamwise and transverse velocity components and the streamwise velocity fluctuations at two different downstream locations ($x/D = 1.5, 2.5$) over a one half of the wake are shown in Figs. 8 to 10. Following the separation of flow from the front corners of the square cylinder, a pressure drop is observed across the cylinder surface and hence a non-zero form drag and a loss of momentum of fluid in the wake are expected. Thus, the time averaged streamwise velocity is found to be smaller within the wake compared with its free stream value as observed in Fig. 8. The time-averaged velocity profiles at a downstream location of $x/D=1.5$ show the influence of inflow turbulence on the recovery rate as seen in Fig. 8 (a). The increase in the turbulence intensity leads to a slower recovery rate for the streamwise velocity component resulting in a better agreement with the experimental data of Lyn, *et al.* (1995) at a turbulence intensity of 2 percent [Fig. 9 (a)]. The effect of inflow turbulence on the transverse velocity profile seems to be relatively small as illustrated in Fig. 9 (a). A measure of the entrainment of the fluid at the edge of the wake can be derived from the transverse velocity profiles and the extent of the entrainment occurs as the turbulence intensity increases. The plot of the streamwise velocity fluctuations at $x/D=1.5$ [Fig. 10 (a)] shows that the numerical predictions of the fluctuations for each case are significantly higher than the experimental measurements. The higher fluctuations for each case can be attributed to the short spanwise length ($4D$) used for the present computations. The contour plots of the streamwise velocity fluctuations clearly show nonzero values with a single peak and there is a decrease in velocity fluctuations as the turbulence intensity increases as seen in Fig. 10 (a). This is probably due to the extent of the entrainment leading to stronger interactions of the separated shear layers and hence the increased diffusion as the inflow turbulence intensity increases. The transverse locations at which the fluctuations attain maximum values are not equal for each case, with differences observed in their respective peak values. The effect of the inflow turbulence on the velocity components and the streamwise normal stress are also shown at a downstream location of $x/D = 2.5$ in Figs. 8 (b) – 10(b). The time-averaged streamwise velocity profile is still not uniform [Fig. 8 (b)] and the minimum velocity at the centreline increases compared to that of downstream location of $x/$

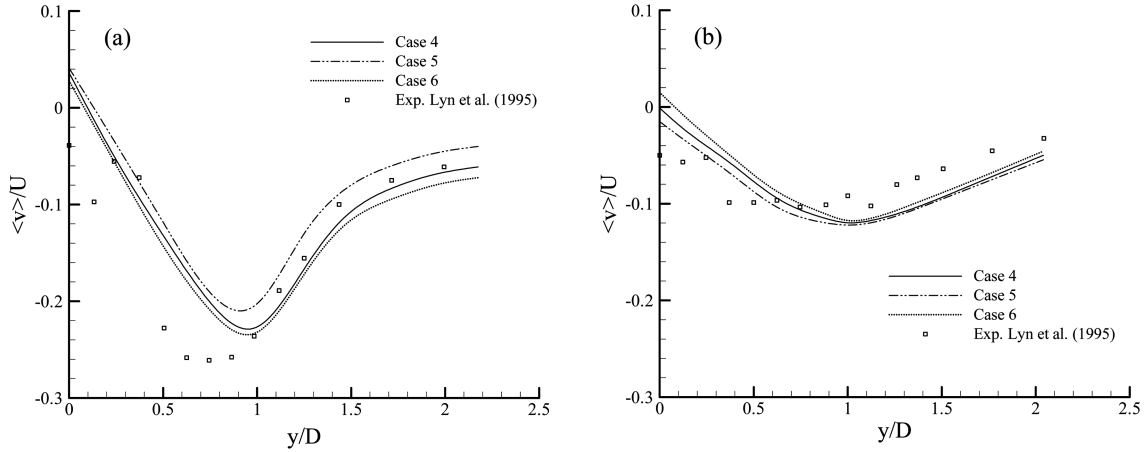


Fig. 9 The time-averaged profiles of transverse velocity component at two different downstream locations in the near wake for different inflow turbulence data; a) Transverse velocity component at $x/D = 1.5$; b) Transverse velocity component at $x/D = 2.5$

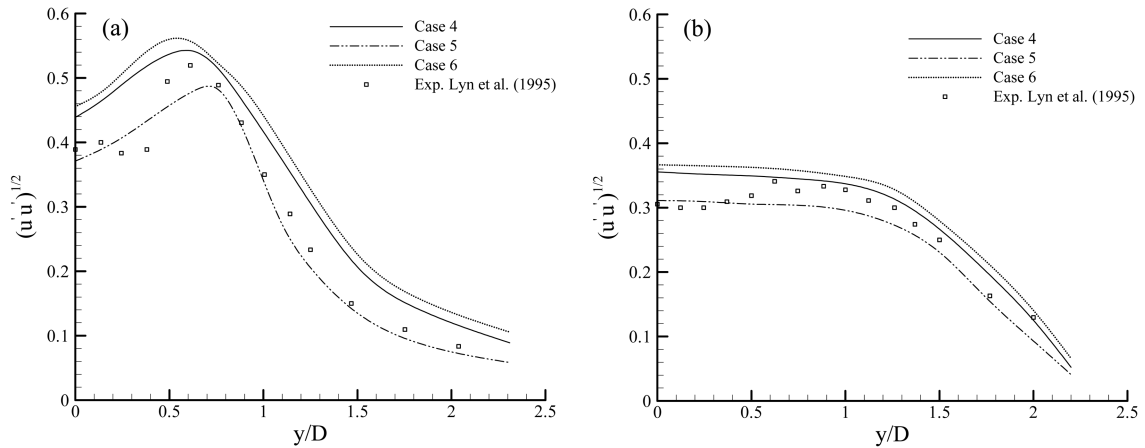


Fig. 10 The time-averaged profiles of streamwise velocity fluctuations at two different downstream locations in the near wake for different inflow turbulence data; a) streamwise velocity fluctuations at $x/D = 1.5$; b) streamwise velocity fluctuations at $x/D = 2.5$

$D = 1.5$. The slower velocity recovery rate is still observed at this location as the inflow turbulence increases. The plots of transverse velocity and the streamwise velocity fluctuations as seen in Figs. 9 (b) and 10 (b) respectively indicate that the inflow turbulence continues to modify the wake at this location in association with the entrainment of the fluid at the edge of the wake.

The turbulence effects on the time averaged pressure distribution are investigated and the results are illustrated in terms of the streamwise profiles of the time averaged pressure coefficient, \overline{C}_p in Fig. 11. The experimental data of Lyn, *et al.* (1995) are also included for a comparison. It is clearly seen in the figure that an increase in the turbulence intensity causes a decrease in the magnitude of \overline{C}_p . This is primarily due to progressively greater interference of the after body of the cylinder with the free shear layers with the increasing turbulence intensity. The extent of the entrainment of the

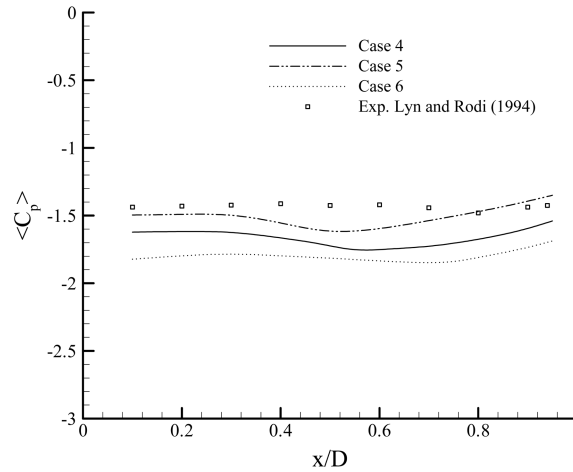


Fig. 11 The streamwise profiles of the time-and-spanwise-averaged streamwise pressure coefficient, $\langle C_p \rangle$ over the cylinder surface for different turbulent inflow data (Cases 4-6) and that of experimental data of Lyn and Rodi (1994). x is measured from the leading edge of the cylinder

fluid from the recirculation region to free shear layers with the increasing turbulence intensity causes an increasing pressure rise (Case 5) along the side surfaces towards the back of the cylinder as observed in Fig. 11 and this leads to higher base pressure and lower drag as summarized in Table 1. The more completed pressure recovery obtained from Case 5 with 10 percent inflow turbulence compared to the other two cases can be attributed to the temporary reattachment of the separated shear layers on the cylinder surface. The inflow turbulence also reduces the r.m.s lift fluctuations, $\overline{C_L}$ occurring near the vortex shedding frequency by disturbing the regularity and spanwise correlation of the shedding as previously suggested by Gartshore (1984)

Figs. 12 (a) to (c) illustrate the instantaneous vorticity contours at the mid-spanwise plane of $z/D = 2$ for different inflow turbulence levels. It is evident from Figs. 12 (a) to (c) that the degree of inflow turbulence has significant effects on the length of the two separated shear layers and the size of the vortex formation region. As the turbulence intensity increases, the increasing entrainment of the fluid from the recirculation zone into the free shear layers increases their curvature towards the sides of the cylinder as previously noted by Huot, *et al.* (1986). The development of the highly curved shear layers interfering with the back corners of the cylinder leads to reduction of the wake width and hence the extensions of the separated shear layers. The stronger interactions of these layers then reduces the length of the vortex formation region and affects the vortex shedding mechanism to reduce the coherence and the strength of shed vortices. The increasing interference with the sides of the cylinder with the increasing turbulence intensity also influences the size of the reverse flow near the sides and the scale of small eddies in it. Due to different level of interactions of the separated shear layers with varying degree of inflow turbulence, the wake destabilization time for each case becomes different. As a result of this, the phase lag occurs in the formation of the large vortices behind the cylinder for each case as seen in Figs. 12 (a) - (c). The phase lag can be attributed to the onset of the wake instability leading to modification of the vortex shedding mechanism (the wake fluctuates more at low inflow turbulence levels). The closer interaction of the two separated shear layers with increasing inflow turbulence level results in early roll-up and shedding of vortices from the cylinder. The wake instability is expected to have an earlier onset for

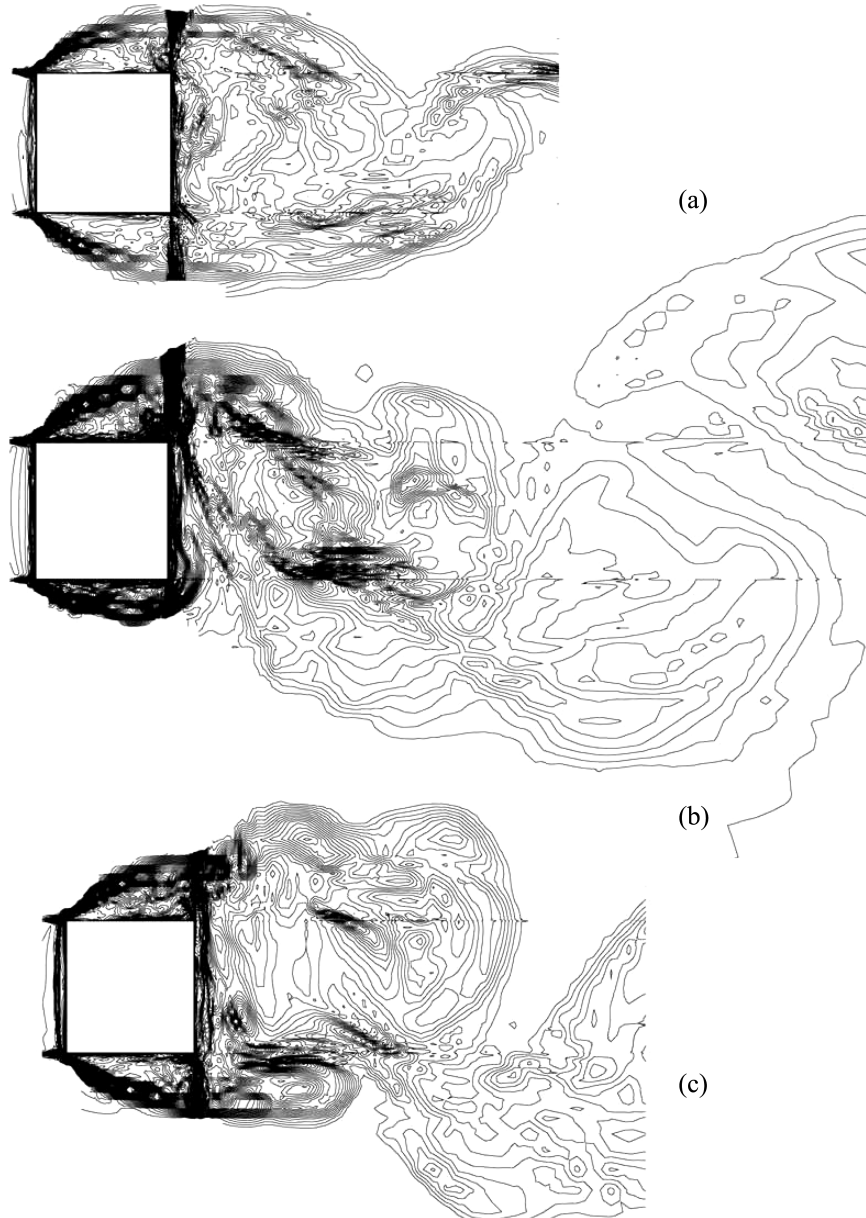


Fig. 12 The instantaneous vorticity contours at the mid-spanwise plane of $z/D = 2$ in the near wake of the cylinder for the 3-D LES computations at a non-dimensional time of $t^* = 54$; a) Case 4; $I_u = 2\%$; b) Case 5; $I_u = 10\%$; c) Case 6; smooth inflow

Case 5 due to higher level of turbulence intensity.

5. Conclusions

The following conclusions can be drawn from the present numerical study:

1. The numerical results show that the use of the present RFG method in conjunction with the LES computations is capable of satisfactorily predicting the effects of inflow turbulence on the flow characteristics in the vicinity of the cylinder surface. Surface pressure distributions, velocity variations, as well as the global features, such as periodic variations of the flow, lift and drag forces, vortex shedding frequency are predicted well by 3-D LES computations in comparison with the available experimental data.
2. The development of turbulent shear layers is considerably influenced by the inflow turbulence. The extent of the entrainment of the fluid from the separation region to free shear layers, the stronger interaction of these layers and the augmentation of the turbulent mixing in the near wake are all observed with the increasing of inflow turbulence intensity.
3. The present turbulent inflow generation method is better suited to 3-D computations compared to 2-D computations for the present LES method due to the fact that the near wake vortex formation mechanism is mainly governed by the 3-D near wake flow characteristics and the 2-D computations are not able to capture the 3-D vortex stretching mechanism and the associated turbulent fluctuations in the near wake. However, the fine mesh resolution in the 2-D plane is still very important.
4. The level of the inflow turbulence has significant influence on the calculation results; in future calculations the optimized conditions for the turbulent inflow data and the modelling aspects for the turbulent properties at the inflow boundary should be carefully studied for engineering flows around high-rise buildings, chimneys, bridges etc.

References

- Akselvoll, K. and Moin, J. (1995), *Large Eddy Simulation of Turbulent Confined Coannular Jets and Turbulent Flow Over a Backward-facing Step*, Report TF-63, Thermosciences Div., Dept. Mech. Eng., Stanford University, Stanford, CA 94305.
- Bechara, W., Bailly, C. and Laton, P. (1994), "Stochastic approach to noise modelling for free turbulent flows", *AIAA Journal*, **32**(3).
- Bosch, G. and Rodi, W. (1998), "Simulation of vortex shedding past a square cylinder with different turbulence models", *Int. J. Numer. Methods Fluids*, **28**, 601-616.
- Bouris, D. and Bergeles, G. (1999), "2D LES of vortex shedding from a square cylinder", *J. Wind Eng. Ind. Aerody.* **80**, 31-46.
- Celik, I. and Shaffer, F. D. (1995), "Long time-averaged solutions of turbulent flow past a circular cylinder", *J. Wind Eng. Ind. Aerody.*, **56**, 185-212.
- Celik, I., Smirnov, A. and Smith, J. (1999), "Appropriate initial and boundary conditions for les of a ship wake", *Proc. of 3rd ASME/JFE Joint Fluids Engineering Conference*, Vol. FEDSM99-7851, San Francisco, California
- Fluent, *FIDAP Users Manual*, 1993.
- Franke, R. and Rodi, W. (1991), "Calculation of vortex shedding past a square cylinder with various turbulence models", *8th Symposium on Turbulent Shear Flows*, Technical University of Munich.
- Gartshore, I. S. (1994), "Some effects of upstream turbulence on the unsteady lift forces imposed on prismatic two dimensional bodies", *J. Fluids Eng.-Transactions of the ASME*, **106**, 418-424.
- Grigoriadis, D. G. E., Bartzis, J. G. and Goulas, A. (2003), "LES of the flow past a rectangular cylinder using the immersed boundary concept", *Int. J. Num. Methods Fluids*, **41**, 615-632.
- Huot, J. P., Rey, C. and Arbet, H. (1986), "Experimental analysis of the pressure field induced on a square cylinder by a turbulent flow", *J. Fluid Mech.*, **162**, 283-298.
- Kondo, K., Mochida, A. and Murakami, S. (1996), "LES computation of isotropic turbulence based on generated inflow turbulence", *Proc. of 14th symposium on Wind Engineering*, December, Japan, 227-232.
- Kondo, K., Murakami, S. and Mochida, A. (1997), "Generation of velocity fluctuations for inflow boundary conditions of LES," *J. Wind Eng. Ind. Aerody.*, **67-68**, 51-64.

- Kraichnan, R. H. (1970), "Diffusion by a random velocity field", *Phys. Fluids*, **13**, 22-31.
- Lee, S. (1997), "Unsteady aerodynamic force prediction on a square cylinder using $k-\varepsilon$ turbulence models", *J. Wind Eng. Ind. Aerody.* **67-68**, 79-90.
- Lee, S., Lele, S. K. and Moin, P. (1992), "Simulation of spatially evolving turbulence and the applicability of Taylor's Hypothesis in compressible flow", *Phys. Fluids*, **A (4)**, 1521-1530.
- Lund, T. S., Wu, X. and Squires, K. D. (1998), "Generation of turbulent inflow data for spatially developing boundary layer simulations", *J. Comput. Physics*, **140**, 233-258.
- Lyn, D. A. and Rodi, W. (1994), "The flapping shear layer formed by flow separation from the forward corner of a square cylinder", *J. Fluid Mech.* **267**, 353-376.
- Lyn, D. A., Einav, S., Rodi, W. and Park, J. H., "A laser-Doppler velocimetry study of ensemble-averaged characteristics of the turbulent near wake of a square cylinder", *J. Fluid Mech.*, **304**, 285-319.
- Maruyama, T. and Morikawa, H. (1994), "Numerical simulation of wind fluctuation conditioned by experimental data in turbulent boundary layer", *Proc. of 13th Symposium on Wind Engineering*, December, 573-578.
- Mochida, A., Murakami, M., Shoji, Y. and Ishida, Y. (1992), "Numerical simulation of flow field around Texas Tech building by large eddy simulation," *Proc. 1st Int. Symposium on Computational Wind Engineering*, Tokyo.
- Murakami, S., Iizuka S. and Ooka, R. (1999), "CFD analysis of turbulent flow past square cylinder using dynamic LES", *J. Fluids Struct.*, **13**, 1097-1112.
- Rai, M. M. and Moin, P. (1993), "Direct numerical simulation of transition and turbulence in a spatially evolving boundary layer", *J. Comput. Physics*, **109**, 162-192.
- Rodi, W., Ferziger, J. H., Breuer, M. and Pourquie, M. (1997), "Status of large eddy simulation: results of workshop", *J. Fluids Eng. Transactions of ASME*, **119**, 248-262.
- Saha, A. K., Muralidhar, K. and Biswas, G. (2000), "Experimental study of flow past a square cylinder at high Reynolds numbers", *Exp. Fluids*, **29**, 553-563.
- Sakamoto, S., Murakami, S. and Kato, A. (1990), "Numerical study on air flow around 2d square prism (part 1) influence of inflow turbulence on surface wind pressure, *Proc. AIJ Annual Meeting*, 99-100.
- Sakamoto, S., Murakami, S. and Mochida, A. (1993), "Numerical study on flow past 2D square cylinder by large eddy simulation: Comparison between 2D and 3D computations", *J. Wind Eng. Ind. Aerody.* **50**, 61-68.
- Smagorinsky, J. (1963), "General circulation experiments with the primitive equations", *Monthly Weather Review*, **91**, 99-152.
- Smirnov, A., Shi, S. and Celik, I. (2000), "Random flow simulations with a bubble dynamic model", *Proc. of FEDSM00 ASME 2000 Fluids Eng. Division Summer Meeting*, June 11-15, Boston, Massachusetts.
- Smirnov, A., Shi, S., and Celik, I. (2002) "Random flow generation technique in large eddy simulations and particle-dynamics modelling" *J. Fluids Eng. -Transactions of ASME*, **123**, 359.
- Spain, B. (1965), *Tensor Calculus*, Oliver and Boyd.
- Spalart, P. R. (1988), "Direct simulation of a turbulent boundary layer up to $Re_\theta = 1410$ ", *J. Fluid Mech.*, **187**, 61.
- Tutar, M. (1998), "Computational modelling of vortex shedding from offshore risers", *Ph. D. Thesis*, University of Hertfordshire, UK.
- Tutar, M. and Holdo, A. E. (2001), "Computational modelling of flow around a circular cylinder in sub-critical flow regime with various turbulence models", *Int. J. Numer. Methods Fluids*, **35**, 763-784.
- van Driest, E. R. (1956), "On the turbulent flow near a wall", *J. Aeronautical Sciences*, **23**, 1007-1011.
- Wakes, S. J., Holdo, A. E. and Tutar, M. (1999), "The role of the near wall function in large eddy simulation in large eddy simulations of bluff body flows", *Proc. of 1999 ASME/JSME Fluids Engineering Division Summer Meeting*, July 18-23, San Francisco.
- Werner, H. and Wengle, H. (1991), "Large eddy simulation of turbulent flow over and around a cube in a plate channel", *Proc. of 8th Symposium on Turbulent Shear Flows*, 155-168.
- Zhou, O. and Leschziner, M. (1991), "A time-correlated stochastic model for particle dispersion in anisotropic turbulence", *Proc. in 8th Turbulent Shear Flows Symposium*, Munich.